Science Advances
AAAS

advances.sciencemag.org/cgi/content/full/4/6/eaao4631/DC1

Supplementary Materials for

Deep-biosphere methane production stimulated by geofluids in the Nankai accretionary complex

Akira Ijiri, Fumio Inagaki, Yusuke Kubo, Rishi R. Adhikari, Shohei Hattori, Tatsuhiko Hoshino, Hiroyuki Imachi, Shinsuke Kawagucci, Yuki Morono, Yoko Ohtomo, Shuhei Ono, Sanae Sakai, Ken Takai, Tomohiro Toki, David T. Wang, Marcos Y. Yoshinaga, Gail L. Arnold, Juichiro Ashi, David H. Case, Tomas Feseker, Kai-Uwe Hinrichs, Yojiro Ikegawa, Minoru Ikehara, Jens Kallmeyer, Hidenori Kumagai, Mark A. Lever, Sumito Morita, Ko-ichi Nakamura, Yuki Nakamura, Manabu Nishizawa, Victoria J. Orphan, Hans Røy, Frauke Schmidt, Atsushi Tani, Wataru Tanikawa, Takeshi Terada, Hitoshi Tomaru, Takeshi Tsuji, Urumu Tsunogai, Yasuhiko T. Yamaguchi, Naohiro Yoshida

Published 13 June 2018, *Sci. Adv.* **4**, eaao4631 (2018)
DOI: 10.1126/sciadv.aao4631

The PDF file includes:

- References (*61–79*)

Other Supplementary Material for this manuscript includes the following:
(available at advances.sciencemag.org/cgi/content/full/4/6/eaao4631/DC1)

- table S1 (Microsoft Excel format). Geochemical data from KMV#5 analyzed in this study.
- table S2 (Microsoft Excel format). $\delta^{13}C\text{-}CH_4$, $\delta D\text{-}CH_4$, and $\Delta^{13}CH_3D$ temperature of Hybrid-PCS sediment core samples.
- table S3 (Microsoft Excel format). Production test of gasses from Hybrid-PCS sediment core samples.
- table S4 (Microsoft Excel format). Cell concentration in sediment core samples from KMV#5.
- table S5 (Microsoft Excel format). Diversity indices of microbial communities in sediment core samples from KMV#5 based on 16*S* rRNA gene sequence analysis.
- table S6 (Microsoft Excel format). Activity of methanogenesis, acetogenesis, and hydrogenase based on radiotracer incubation analyses.
- table S7 (Microsoft Excel format). Concentration of archaeal core and IPLs.
- table S8 (Microsoft Excel format). Thermogenic and biogenic end-member values for mixing calculation.

Supplementary Text

I. Implication for the occurrence of thermophilic microbial communities in the deep and old accretionary prism

In the lipid biomarker analysis of deep mud-volcano core samples, we detected H-shaped GDGTs (table S7); these were also observed with one to three additional methyl groups in the isoprenoidal chain (cf. ref. *40*). The H-shaped GDGTs are diagnostic biomarkers for thermophilic and hyperthermophilic archaea, including methanogens (*61*), Thermococcales (*62*) and Thermoplasmatales (*63*), and have been exclusively detected in hydrothermal settings (*40*). The distribution of H-shaped GDGTs with dominant core and monoglycosidic species implies that these are fossil signals of thermophilic or hyperthermophilic archaea. Considering the fact that the concentrations of H-shaped GDGTs were relatively variable throughout the sediments, and the water in the original mud reservoir was mainly supplied from dehydration of clay minerals (that is, the smectite-illite reaction), detection of H-shaped GDGTs suggest that (hyper)thermophilic archaea may be present in the deeper and hotter realm of the old accretionary prism.

Controversially, 16S rRNA gene analysis showed that most sequences were related to psychrophilic amd mesophilic members that have been often observed in cold to warm subseafloor sediments (Fig. 5, B and C). This is consistent with these members being derived from mesophilic microbial communities inhabiting the original mud reservoir in the lower sedimentary basin, where the *in situ* temperature was expected to be 17°C to 30°C (see the main text). Nevertheless, among 436,687 sequence reads, we detected 48 sequences related to Aquificales (1 and 47 sequences from 104 and 119 mbsf, respectively), 3 sequences of Thermotogales at 119 mbsf, and 1 sequence of Thermales at 2.58 mbsf, which are very minor but presumably thermophilic or hyperthermophilic bacterial members based on the phylogenetic placement. We suggest that these signals are related to fossil or inactive thermophilic bacteria in the modern deep mud-volcano biosphere.

II. Isolation and characterization of methanogenic archaeon strain 1H1

We set up 240 culture vessels in total for cultivation of methanogens from the KMV#5 core samples: 6 sediment core samples, 2 types of media, 5 methanogenic substrates, 2 cultivation temperatures, duplicate for each substrate (see Supplementary Methods). Cell growth and methanogenesis were observed in only three cultures after 9 months of incubation. These three cultures were from Site C9005 sediment sample using the 1:10-diluted MJ medium (NaCl concentration: 3 g l^{-1}). No enrichment cultures were obtained from Site C9004 sediment samples, even after 1 year of incubation. The methanogenic substrates of the enrichment cultures were H_2/CO_2, methanol and trimethylamine. Microscopic observation showed that the enrichment culture consisted of irregular coccoid-shaped cells that produced F_{420}-like auto-fluorescence, indicating the growth of methanogens. All enrichment cultures were transferred to fresh medium with 10% (v/v) inoculation. Subsequently, only a H_2/CO_2-fed culture was successively transferred. To isolate the methanogen, a serial dilution technique was used in both liquid and solid media supplemented with H_2/CO_2 as the sole energy source. Finally, we obtained a pure culture of methanogen, strain 1H1.

Cells of strain 1H1 were non-motile, irregular cocci, 0.8–1.8 µm in diameter (fig. S7, A and B). Strain 1H1 utilizes H_2/CO_2, acetate, methanol, dimethylamine, and trimethylamine for growth and methanogenesis. The following substrates did not support growth and methane production: formate, dimethylsulfide, ethanol, 1-propanol, 2-propanol, cyclopentanol, 1-butanol, and 2-butanol. Yeast extract and acetate were not required for growth. Strain 1H1 grew at temperatures of between 2°C and 50°C with optimum growth at 40°C (fig. S7C). Although the strain was cultured from the marine subsurface, it was found to preferentially grow under low NaCl concentrations (down to 0 g l^{-1}) (fig. S7D). In addition, the strain had a wide range of NaCl concentrations at which it is capable of growth (NaCl concentration: 0–70 g l^{-1}).

Comparative 16S rRNA gene sequence analysis showed that strain 1H1 was affiliated with the genus *Methanosarcina* (fig. S7). The sequence was identical with those of some *Methanosarcina mazei* strains. The strain has been deposited in the Japan Collection for Microorganisms (JCM 19936).

III. Assumption of thermogenic and biogenic end member values for mixing calculation based on the data from the Nankai Trough area

The calculation of mixing biogenic and thermogenic CH_4 at KMV#5 requires estimation of $\delta^{13}C$ and δD of CH_4 and C_1/C_2 ratio from biogenic and thermogenic end-members as inputs. We used previously reported data from nearby sites to constrain these inputs (fig. S8A). The assumed biogenic and thermogenic end-member values for the mixing calculations are shown in table S8.

Biogenic end-member

We estimated the $\delta^{13}C_{CH4}$ value of the biogenic end-member using the average $\delta^{13}C_{DIC}$ below 5 mbsf at the KMV#5 measured in this study (+40‰) and the difference between $\delta^{13}C_{CH4}$ and $\delta^{13}C_{DIC}$ ($\varepsilon_c \approx \delta^{13}C_{DIC} - \delta^{13}C_{CH4}$, which is between 80‰ and 69‰) (*14*) in the active methanogenesis zone between the SMTZ (~2 mbsf) and ca. 80 mbsf at Sites C0001, C0002, C0004, and C0008 (*55*) (fig. S8B). Our estimated $\delta^{13}C_{CH4}$ of biogenic end-member is higher than typical biogenic CH_4 (< –60‰; ref. *12*), because CH_4 at this site is inferred to derive from highly ^{13}C-enriched DIC (see main text). The C_1/C_2 ratio of the biogenic end-member was estimated based on the average values in the active methanogenesis zone at Sites C0001, C0004, and C0008 (*55*) (fig. S8C). We assumed that the average C_1/C_2 ratio (i.e., 3500) in the active methanogenesis zone at these sites is the most plausible biogenic end-member value, and the observed range of 2000–6200 is the possible range of the biogenic end-member. We assumed that the most plausible δD_{CH4} of biogenic end-member is –166‰ which is observed at the Kumano basin and the possible values are between –188‰ and –166‰ (*44*, *64*).

Thermogenic end-member

The $\delta^{13}C_{CH4}$ and C_1/C_2 ratio of thermogenic end-member is based on data from MITI Well off Tokai (*65*), Site 808 off Muroto (*64*), and Sagara oil field (*66*) (Fig. 4A and fig. S8A–C). Although the referred sites are located far from each other and the source rock and thermal conditions are different, these data indicate that the $\delta^{13}C_{CH4}$ values and C_1/C_2 ratios of the thermogenic gases in the Nankai Trough area fall within a narrow range ($\delta^{13}C_{CH4}$: –45‰ to –40‰; C_1/C_2: 8 to 11). Therefore, we assumed that the $\delta^{13}C_{CH4}$ value and C_1/C_2 ratio of the thermogenic end-member falls within the range, and those of thermogenic gas below 2100 mbsf at the MITI Well ($\delta^{13}C_{CH4}$: –40‰; C_1/C_2: 8), which is the site closest to the Kumano basin, are most plausible values of the thermogenic end-member. In the Nankai Trough area, the δD of reliable thermogenic CH_4 has been measured only at Site 808 off Muroto (*64*). At Site 808, δD_{CH4} values of the thermogenic CH_4 below 1100 mbsf (>90°C) were –233‰ and –225‰. The δD values there are typical of CH_4 generated at an early stage of thermal maturity (*13*). For our mixing curves, we assumed that the possible range of δD_{CH4} of the thermogenic end-member is –229 to –138‰. The latter (maximum) value accounts for a possible contribution from higher-maturity gases. The lowest temperature for the production of thermogenic gas was assumed to be 80°C based on data from Site C0002 in the Kumano basin. At the IODP Site C0002, which was penetrated down to ~2 km below seafloor at 81–85°C, the mixed thermogenic gas at this horizon is delivered from deeper and thus hotter realms and no *in situ* production of thermogenic gas occurs (*44*). Therefore, we infer that the production of the thermogenic gas does not occur below 80°C. The maximum temperature was assumed to be ~220°C based on previous predictions, according to which the most gas is formed between 150°C and 220°C (*67*).

Supplementary Methods

Calculation of methane hydrate-saturation based on $\delta^{18}O_{H2O}$ and δD_{H2O}

Methane hydrate-saturation was calculated from the measured oxygen and hydrogen isotopic compositions of water ($\delta^{18}O_{H2O}$ and δD_{H2O}) and the original $\delta^{18}O$ and δD values of pore water before the formation of methane hydrates, according to the procedure described in Tomaru *et al.* (*68*). The original $\delta^{18}O$ and δD values are estimated to be +4.3 to +5.3‰ and –9.2 to –16.2‰, respectively, based on the averaged $\delta^{18}O$ and δD of hydrate water and known isotopic fractionation factors of oxygen and hydrogen in water between Structure I-gas hydrate and liquid water, which are 1.0024–1.0034 and 1.017–1.024, respectively (*69*). Using Raman spectroscopy, the formation structure of methane hydrate-chunks, which were obtained from 2.9 mbsf and immediately stored in a liquid N_2 tank onboard, was determined to be "Structure I" due to the C-H symmetric stretch of CH_4 corresponding to large and small cages (fig. S1). The addition of ^{18}O- and D-enriched hydrate water by the dissociation of hydrates during core recovery and sampling should result in higher $\delta^{18}O_{H2O}$ and δD_{H2O} values than the estimated $\delta^{18}O$ and δD values of the original pore water. Based on the isotopic difference between pore water sample and original pore water, we determined the volume fraction between added gas hydrate-dissociated water and pore water *M* using the following equation

$$M = (\delta_{H2O} - \delta_O) / (\delta_h - \delta_O) \quad (1)$$

where δ_{H2O} and δ_O represent measured values of $\delta^{18}O$ or δD of pore water, and the isotopic compositions of original pore water before methane hydrate precipitation, respectively, and δ_h represents $\delta^{18}O$ of the hydrate sample.

One mole of methane hydrate with the stoichiometric composition $CH_4 \cdot 5.75H_2O$ (M = 119.5 g) contains 103.5 g of water, and has a density of 0.91 g cm^{-3} (*70*). Hence 103.5 cm^3 of hydrate-dissociated water is derived from 131.3 (= 119.5/0.91) cm^3 of gas hydrate. That is, one volume of pure water generates 1.27 volumes of gas hydrate. The gas hydrate saturation *Sh* is then calculated as follows

$$Sh = 1.27M / (1 + 0.27M) \times 100\ (\%) \quad (2)$$

Figure S4, A and B show the vertical profiles of estimated methane hydrate-saturation in pore space. Because the estimated $\delta^{18}O$ and δD values of original pore water vary from +4.3‰ to +5.3‰ and from -9.2‰ to –16.2‰, respectively, and given the range of reported isotopic fractionation factors of oxygen and hydrogen in water between Structure I-gas hydrate and liquid water (*69*), the estimates of methane hydrate-saturation are associated with 20–30% of relative uncertainty. When we adopted larger isotope fractionation to estimate $\delta^{18}O$ and δD values of original pore water, the estimated methane hydrate-saturations sometimes resulted in negative values.

Taxonomic classification of the sequence reads, data processing for OTU picking and beta diversity analysis

The obtained sequence reads were processed as described elsewhere (*56*). All the sequence reads were processed using Pipeline Initial Process (http://pyro.cme.msu.edu/init/form.spr) with the following parameters: forward primer maximum edit distance, 2; maximum number of *N* = s, 0; minimum average exponential quality score, 20; reverse primer maximum edit distance, 0; and minimum sequence length,

150. For the classification and screening of the processed sequences, a BLAST+ analysis using the SILVA database (http://www.arb-silva.de) was conducted. The mothur software package (https://www.mothur.org) was used to remove chimeric sequences and to cluster the sequence reads into OTUs with a 97% sequence similarity threshold. Using the defined OTUs, Bray-Curtis dissimilarity distance of the microbial communities was calculated and average-linkage clustering analysis was conducted using the mothur package.

Using the abundance of top 100 OTUs at different depths, Spearman's rank correlation coefficient was calculated. Network analysis and visualization was performed by Cytoscape version 3.2.0 using the Spearman's rank correlation coefficient larger than 0.7.

PCR amplification of methyl co-enzyme M reductase genes

Using the environmental DNA extracted from the mud-volcano core samples as the PCR template, we tried to amplify methyl co-enzyme M reductase (*mcrA*) genes for methanogenic archaeal communities. We used general *mcrA*-targeting primers mcrIRD F and mcrIRD R (*71*). PCR mix consisted of 1 × MightyAmp buffer (Takara bio), 0.3 µM of each primer, 0.5 U of MightyAmp DNA polymerase, and 1.0 µl of the extracted DNA solution, in a 20-µl volume. After initial denaturation at 98°C for 2 min, 40 cycles of PCR were carried out with denaturation at 98°C for 10 min, annealing at 56°C for 15 s, and elongation at 68°C for 30 s. Because no amplification products were obtained after the PCR, we tried to amplify the extracted DNA by multiple displacement amplification before PCR. We tried to amplify *mcrA* gene from the MDA product using the same PCR condition as described above. However, no PCR products of *mcrA* gene were obtained.

Cultivation of methanogens

To cultivate methanogens, we used six whole round core samples obtained from Hole A at Site C9004 and Hole E at Site C9005: samples from the sediment depths of 0.66, 3.99, 12.10, 14.97, 18.10 mbsf (Site C9004) and 12.82 mbsf (Site C9005 located in the upper southwestern slope of the KMV#5 [*49*]). The sediment samples were collected from the innermost portion of the whole round core using a sterile tip-cut plastic syringe in a laminar flow clean bench onboard the *Chikyu*. The sediment samples were preserved in glass bottles under anaerobic condition, and the samples were stored at 4°C in the dark until experiments were performed.

We prepared two types of media for enrichment of methanogens. The first medium (named MJS medium: ref. *72*) consisted of the following components (l^{-1}): 0.125 g NH_4Cl, 0.14 g K_2HPO_4, 0.8 g $CaCl_2 \cdot 2H_2O$, 4.18 g $MgCl_2 \cdot 6H_2O$, 0.33 g KCl, 30 g NaCl, 2.5 g $NaHCO_3$, 0.72 g $Na_2S \cdot 9H_2O$, 10 ml trace mineral solution, 1 ml Se/W solution, 1 ml vitamin solution, and resazurin solution (1 mg ml^{-1}). The trace elemental solution contained (l^{-1}): 0.596 g $FeCl_2 \cdot 4H_2O$, 0.528 g $MnCl_2 \cdot 4H_2O$, 0.083 g $CoCl_2$, 0.085 g $ZnCl_2$, 0.005 g $CuCl_2$, 0.001 g $AlCl_3$, 0.01 g H_3BO_3, 0.01 g $Na_2MoO_4 \cdot 2H_2O$, and 0.259 g $NiCl_2$. The Se/W solution contained (l^{-1}): 1 g Na_2SeO_3, and 0.5 g $Na_2WO_4 \cdot 2H_2O$. The vitamin solution was composed of the following vitamins (l^{-1}): 20 mg biotin, 20 mg folic acid, 100 mg pyridoxine·HCl, 50 mg thiamine·HCl, 50 mg riboflavin, 50 mg nicotinic acid, 50 mg DL-pantothenate (Ca salt), 1 mg vitamin B_{12}, 50 mg *p*-aminobenzoic acid, and 50 mg lipoic acid. The second medium was 1:10-diluted MJS medium, but the medium contained the same amounts of $NaHCO_3$, $Na_2S \cdot 9H_2O$, trace mineral solution, Se/W solution, vitamin solution and resazurin solution. The final pH value of the two media was 7.0 at 25°C. The following each of the methanogenic substrates were added to the medium as the

sole energy source: H_2/CO_2 (approximately 150 kPa in the head space), formate (20 mM), acetate (20 mM), methanol (10 mM), and trimethylamine (10 mM). Just before cultivation, the sediment samples were suspended with the anaerobic media and approximately 15 ml of the sediment slurry were inoculated into each enrichment culture medium bottle. Cultivations for the primary enrichment cultures were performed in 50-ml glass bottles containing 15 ml medium at 20°C and 55°C under anaerobic conditions. The primary enrichment cultures were set up in duplicate for each substrate. The serum vials were sealed with butyl rubber stoppers and aluminum crimp seals.

Isolation and characterization of methanogenic archaeon strain 1H1

Isolation of strain 1H1 from the enrichment cultures (fig. S7) was conducted by serial dilution in liquid medium supplemented with a mixture of antibiotics (vancomycin and kanamycin, the concentration of each was 50 μg ml^{-1}) and roll-tubes. After enrichment, all cultivations were performed using the MJS medium, in which the NaCl concentration was 3 g l^{-1}. Methane concentration was determined by gas chromatography (GC3200G, GL Science) with a thermal conductivity detector.
Cell morphology was examined under a fluorescence microscope (BX51F; Olympus) with a color CCD camera system (DP72; Olympus). Growth and substrate utilization were determined from microscopic observation and production of methane. All incubations for the substrate utilization test were performed using exponentially growing cultures (10% inoculum, by volume) at 40°C for over 1 month. Effects of temperature and NaCl concentration on the growth of strain 1H1 were determined in H_2/CO_2-fed medium. The growth rates were calculated by measuring methane production. To evaluate the temperature range for growth, cultures were incubated at 2, 4, 10, 15, 20, 25, 30, 37, 40, 42, 45, 50 and 55°C (pH 7.0). NaCl requirements were determined with varying concentrations of NaCl from 0 to 80 g l^{-1} in the basal medium. All incubations for these tests were performed in triplicate culture vessels for over 4 months incubation. The 16S rRNA gene sequence of the isolate was determined according to a previous report (*73*). The 16S rRNA gene sequence-based phylogenetic tree reconstruction was performed using the neighbor-joining method with Jukes-Cantor correction, implemented in the ARB program (fig. S7E) (*74*). To estimate the confidence of tree topologies, bootstrap-resampling analysis with 1000 replicates was performed for the neighbor-joining method by using MEGA program version 7 (*75*).

Mixing model for clumped isotopes of methane

The $\Delta^{13}CH_3D$ of a mixture depends on the $\Delta^{13}CH_3D$ of the end-members, as well as the $\delta^{13}C$ and δD values of the end-members (*25*, *47*, *76*). The $\Delta^{13}CH_3D$ of mixture with two-component mixing of end-members (A and B) can be approximated as follows (*47*)

$$\Delta^{13}CH_3D_{mixture} \approx f_A[\Delta^{13}CH_3D]_A+(1–fA)[\ [\Delta^{13}CH_3D]_B + f_A(1–f_A)(\ \delta^{13}C_A–\delta^{13}{}_B)(\delta D_A–\delta D_B) \qquad (3)$$

Clumped isotope data, taken in combination with C_1/C_2 ratios, have been used previously to estimate the relative amounts of biogenic and thermogenic gases (*48*). Assumptions must be made about the biogenic and thermogenic end-member values of δD and $\delta^{13}C_{CH4}$, and their clumped isotope temperatures. In our case, clumped isotope temperature of the biogenic end-member value is unknown. We constrain its plausible range as follows: Assuming two-end-member mixing between biogenic ($\delta^{13}C$: –39.5‰ to –29‰ [most plausible: –39.5‰]; δD: –188‰ to –166‰ [most plausible: –166‰] and thermogenic CH_4 ($\delta^{13}C$: –45‰ to –40‰ [most plausible –40‰]; δD: –229‰ to –138‰ [most plausible: –229‰]), we plot

mixing curves between two end-members (fig. S9). Each of the curves shown corresponds to a mixture that carries a 30°C $\Delta^{13}CH_3D$ temperature, but with a different proportion of biogenic CH_4 and/or different assumed $\Delta^{13}CH_3D$ temperature for the biogenic end-member.

The diagram of mixing curves with various biogenic fractions constrains the fraction of biogenic CH_4 in the mud volcano samples to at least 70% of the total CH_4. The calculated fraction of biogenic methane cannot be less than 70% unless the $\Delta^{13}CH_3D$ temperature of the biogenic end-member is <0°C, which is improbable for the sediment in the Kumano basin, or unless the $\Delta^{13}CH_3D$ temperature of thermogenic methane is <<150°C.

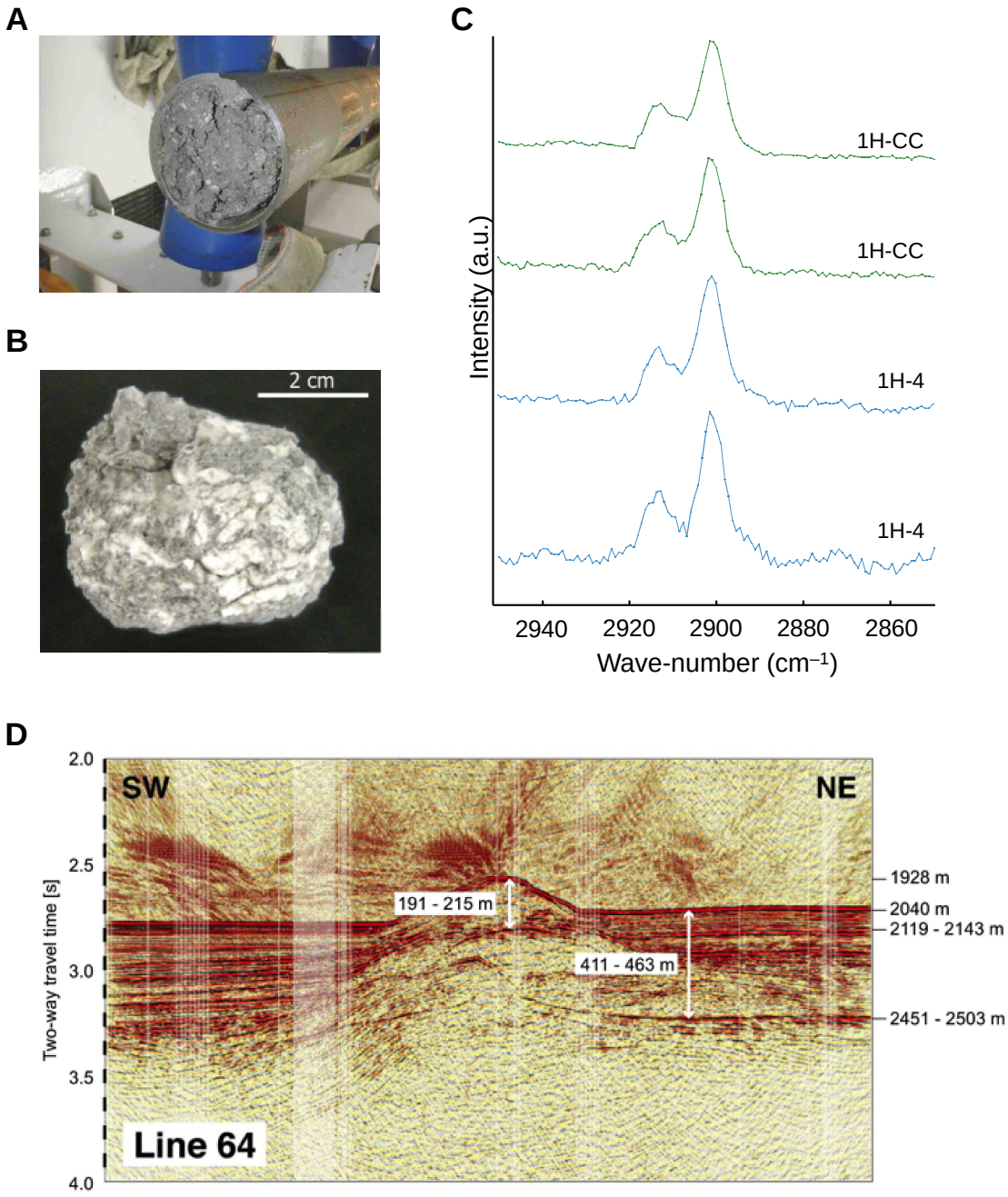

fig. S1. Photographs and Raman spectra of methane hydrate and a seismic profile of KMV#5. (**A**) Photograph of small patchy grains of methane hydrates in the KMV#5 sediment core. (**B**) Photograph of a methane hydrate chunk observed in the sediment core. (**C**) Raman spectra for methane hydrate-chunks collected from the KMV#5. The C-H symmetric stretching bands of methane in small cages (5^{12}) and large cages ($5^{12}6^2$) are indicated at 2915 cm^{-1} and 2905 cm^{-1}, respectively, suggesting the occurrence of "Structure I" methane hydrates in the KMV#5. The Raman intensities were calculated using Lorentzian curve fitting method. (**D**) A SW-NE seismic line across KMV#5 shows a bottom-simulating reflector (BSR) at around 411–463 mbsf in the immediate vicinity of the mud-volcano. Within the mud-volcano, other strong reflectors can be observed at around 191–215 mbsf. Time to depth conversion is based on *P*-wave velocities of 1500 m s^{-1} in the water column, and 1600–1800 m s^{-1} in the sediment.

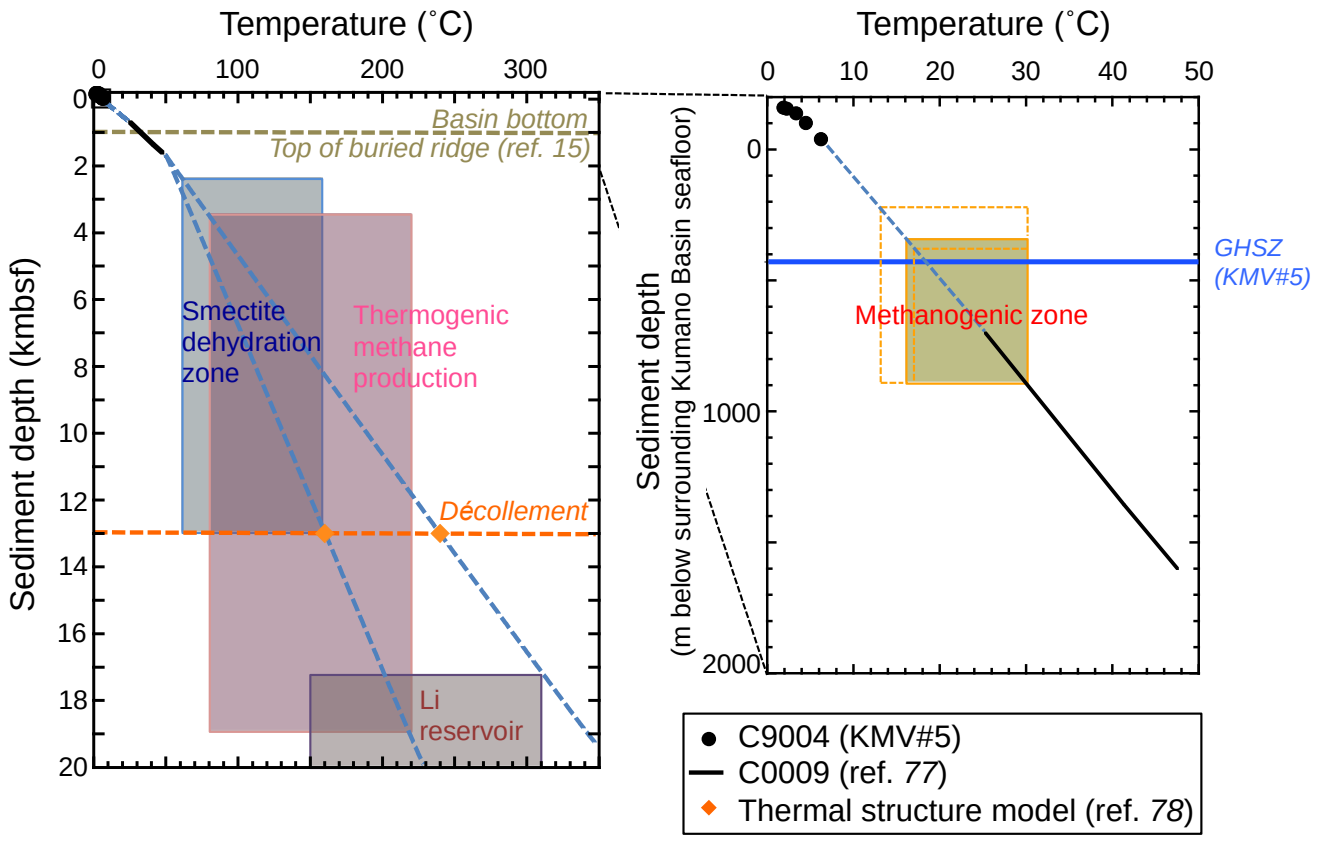

fig. S2. Thermal gradient based on the temperatures measured in situ at KMV#5 and IODP site C0009. The temperature at Site C9004 of KMV#5 was measured by using the APCT-3. The temperature was determined by extrapolation of thermal equilibrium during *in situ* temperature measurement for several minutes. The temperature profile at Site C0009 was calculated based on the heat flow in shallow sediment and the thermal conductivity at C0009 (*77*). Temperature at the décollement is estimated based on the thermal structure model of the Nankai subduction zone (*78*).

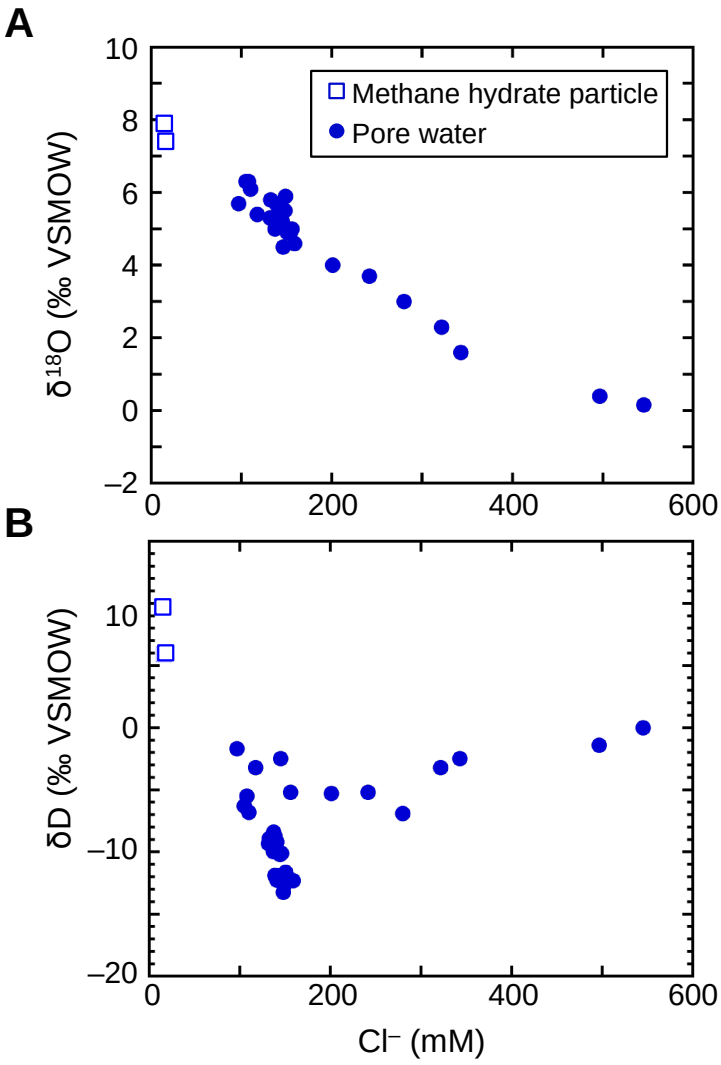

fig. S3. Chloride concentrations versus stable isotopic compositions of water. (**A**) Cl^- concentrations vs. $\delta^{18}O$ values of water. (**B**) Cl^- concentrations vs. δD values of water. Blue dots and squares represent porewater in sediment and water dissociated from a methane hydrate-chunk, respectively.

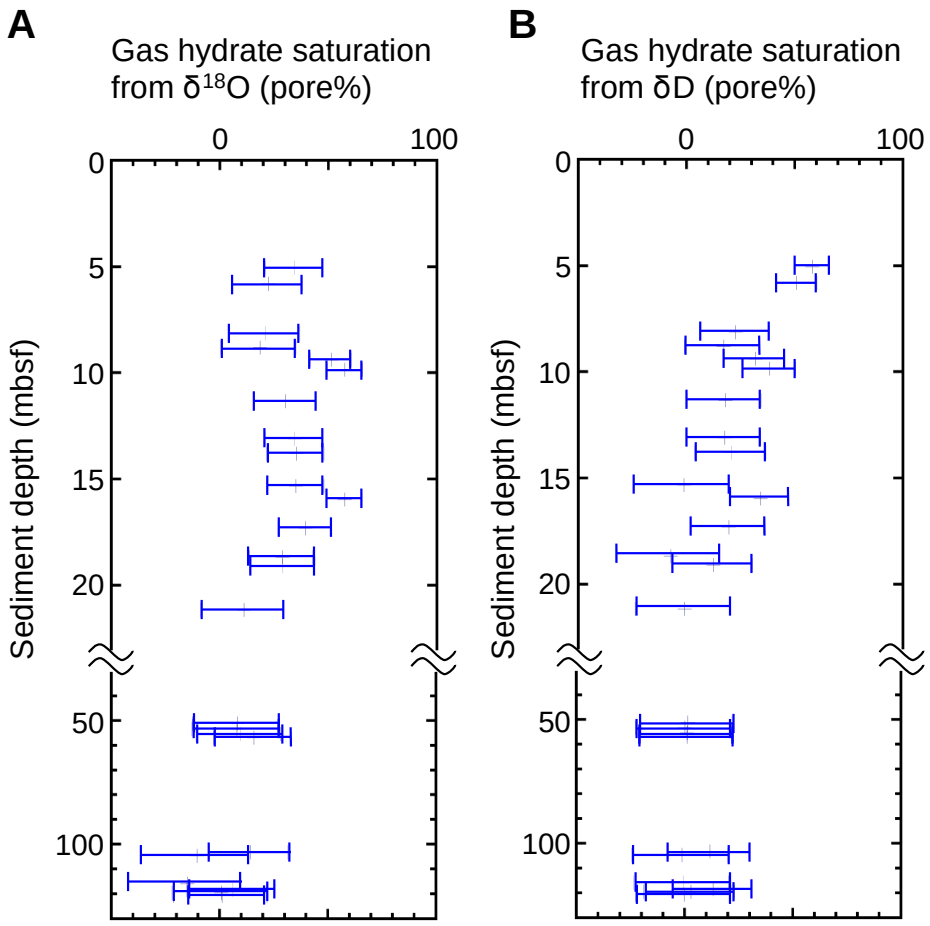

fig. S4. Depth profile of the estimated methane hydrate saturation in pore space based on $\delta^{18}O$ and δD. (**A**) $\delta^{18}O$, (**B**) δD (see Supplementary Methods).

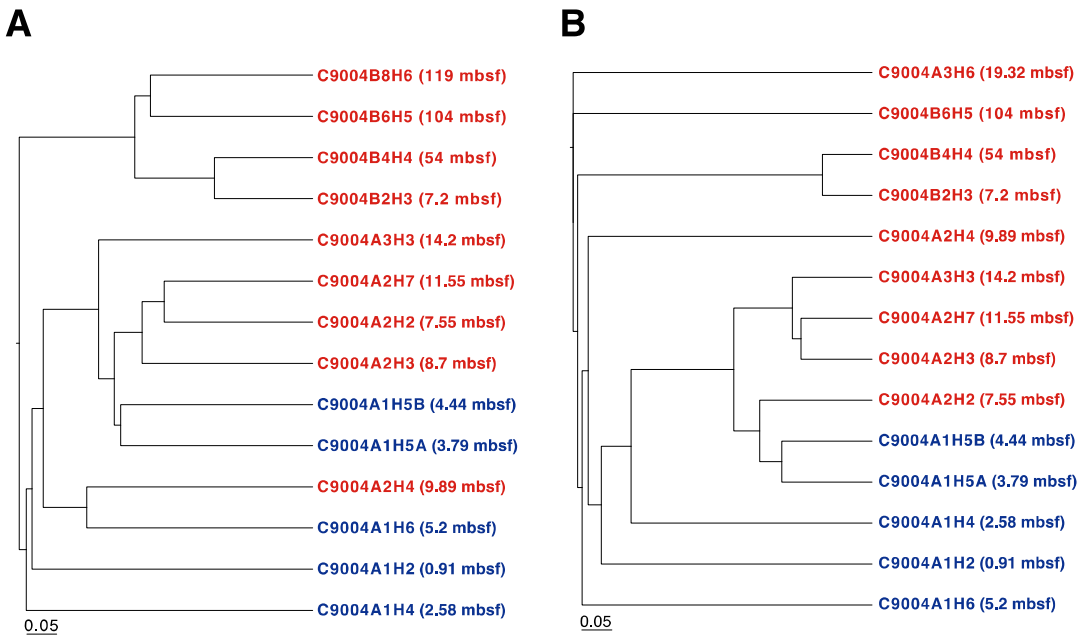

fig. S5. Average linkage clustering analysis based on the Bray-Curtis dissimilarity distance of 16*S* rRNA genes. Clustering of bacterial (**A**) and archaeal (**B**) communities. The Bray-Curtis distance values were calculated based on the operational taxonomic units with 97% similarity cutoff. Blue and red communities represent the depth location above and below 6 mbsf, respectively. Bars indicate square distance of the average linkage clustering.

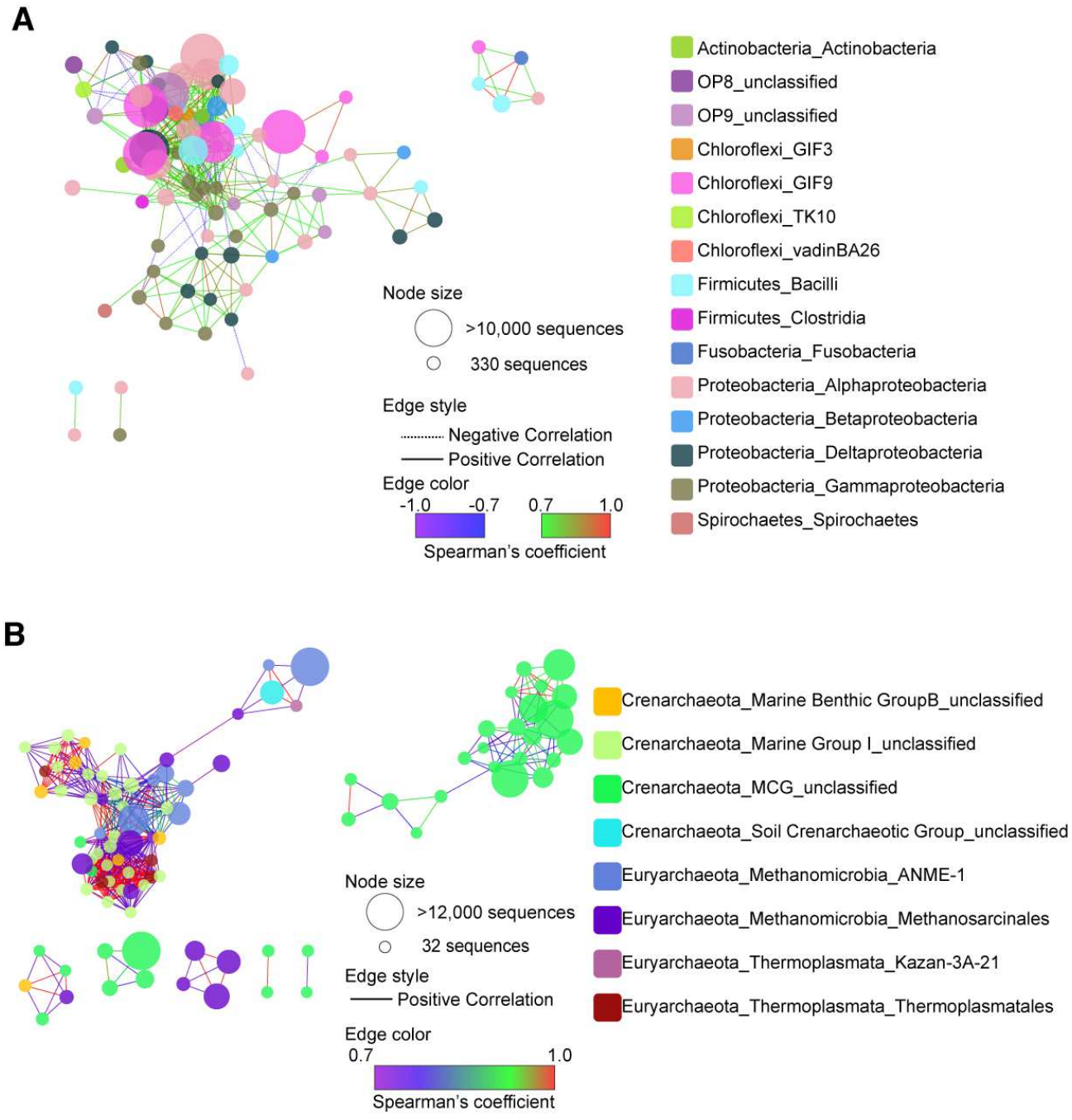

fig. S6. Community network analysis based on Spearman's correlation coefficient. Network graphs for bacterial (**A**) and archaeal (**B**) communities. Spearman's correlation coefficient was determined to identify co-occurrence patterns of OTUs with 95% similarity cutoff. The significant correlations ($p < 0.005$) with coefficient (rho) greater than 0.7 or smaller than –0.7 were used for visualization by Cytoscape as network graph.

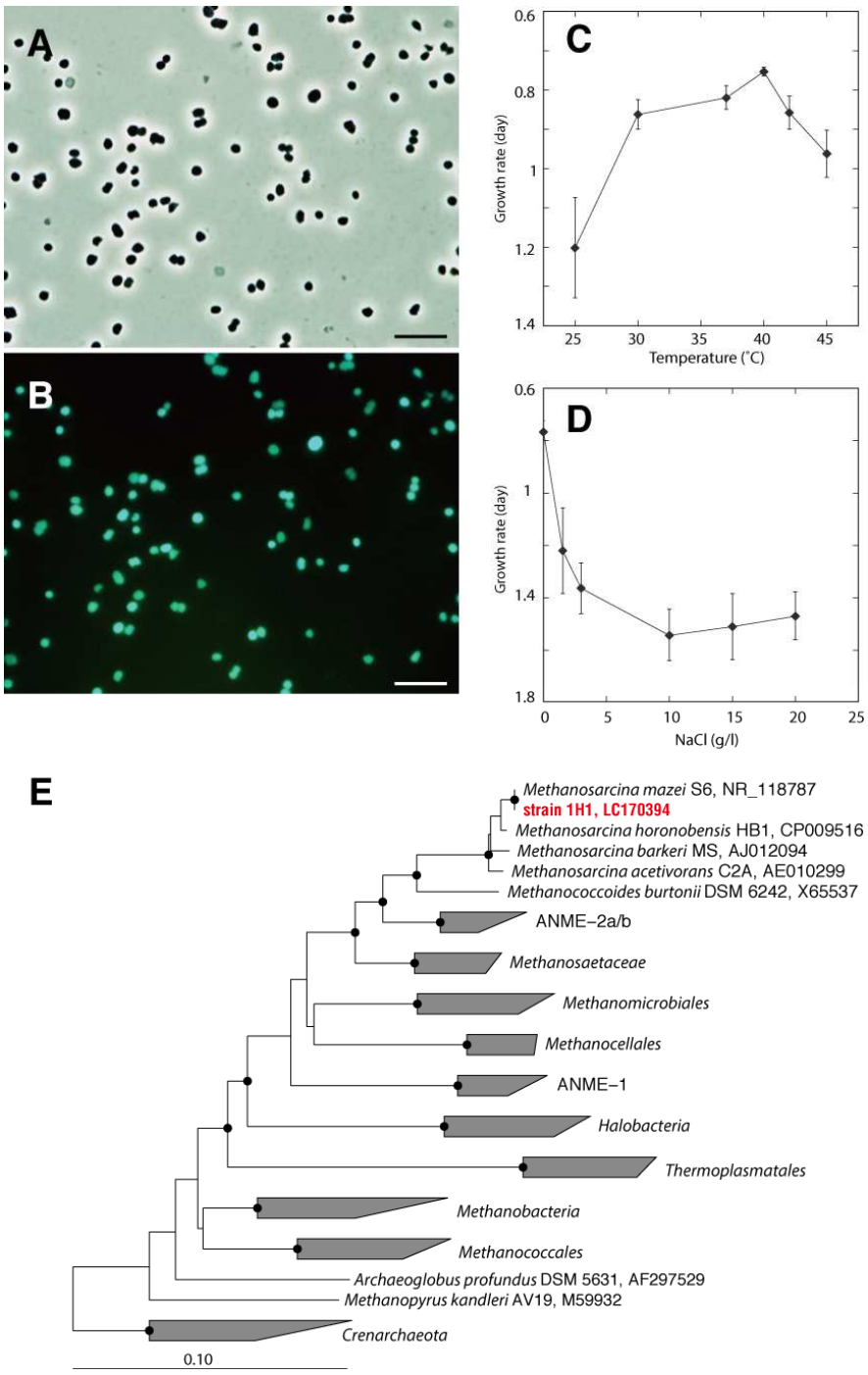

fig. S7. Characteristics of the isolated methanogenic archaeon strain 1H1. (**A**-**B**) Photomicrographs of strain 1H1 grown on H_2/CO_2 medium. Shown are a phase-contrast micrograph (A) and fluorescence micrograph (B) of the same field. Bars represent 10 μm. (**C**-**D**) Effect of temperature and NaCl concentration on growth. Effect of temperature (C) and NaCl concentration (D) on the specific growth rate of strain 1H1 on H_2/CO_2 medium. The specific growth rates were measured only for optimum growth. Error bars indicate standard deviations of triplicate determinations. (**E**) Phylogenetic tree based on 16S rRNA gene sequences showing the placement of strain 1H1. The tree was constructed by using the neighbor-joining algorithm. The bar indicates 0.1 changes per nucleotide sequence position. The solid circles at nodes indicate positions where the confidence value of 1000 bootstrap trials supports more than 80%. Accession numbers are shown after the species/strain names.

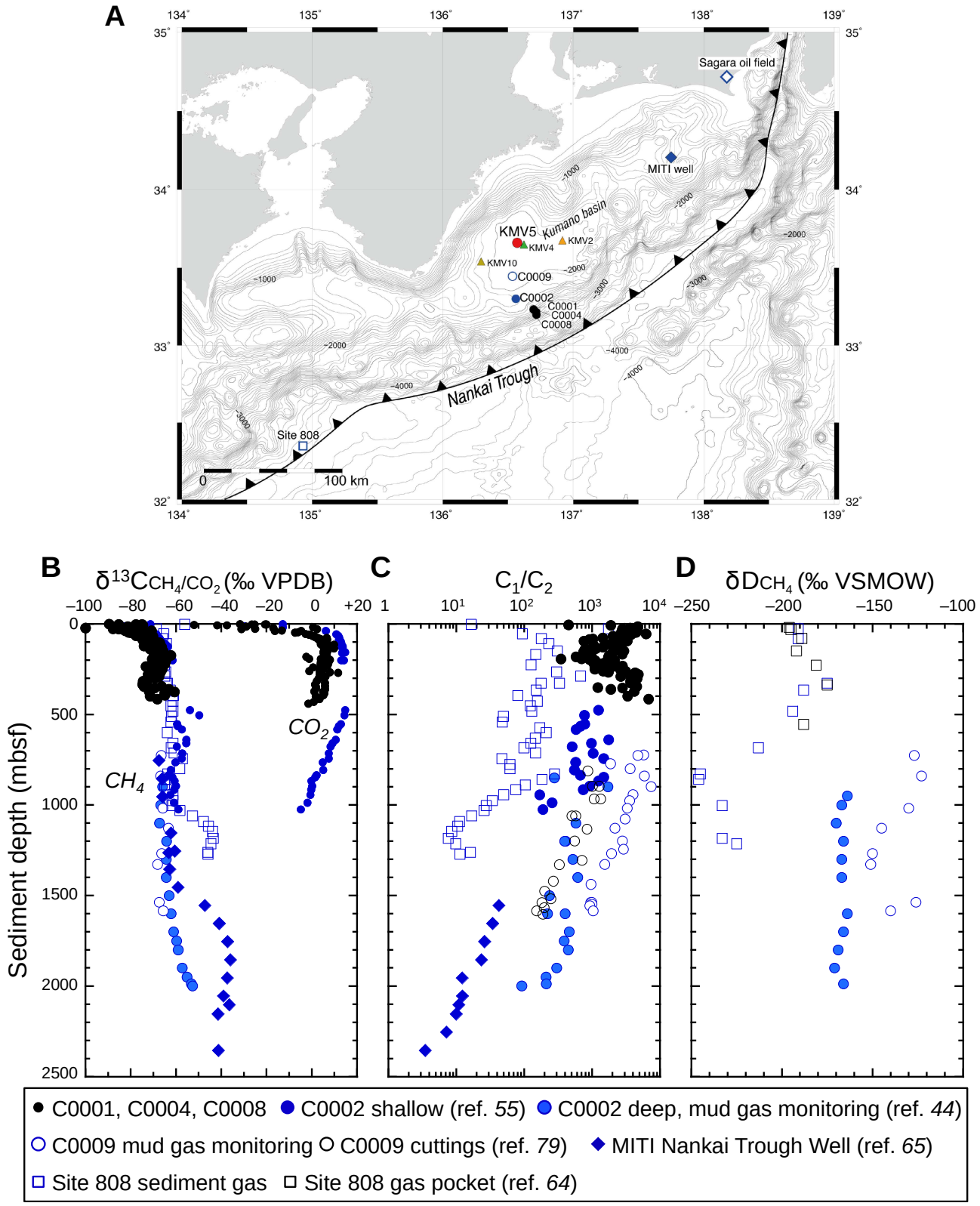

fig. S8. Chemical and stable isotopic compositions of hydrocarbon gases in the Nankai Trough area. (**A**) Locations of the reference sites at which hydrocarbon gas data have been reported (*44*, *55*, *64*, *65*, *66*, *79*). Vertical profiles of $\delta^{13}C_{CH4}$ and $\delta^{13}C_{CO2}$ (**B**), C_1/C_2 ratio (**C**), and δD_{CH4} (**D**) at the reference sites.

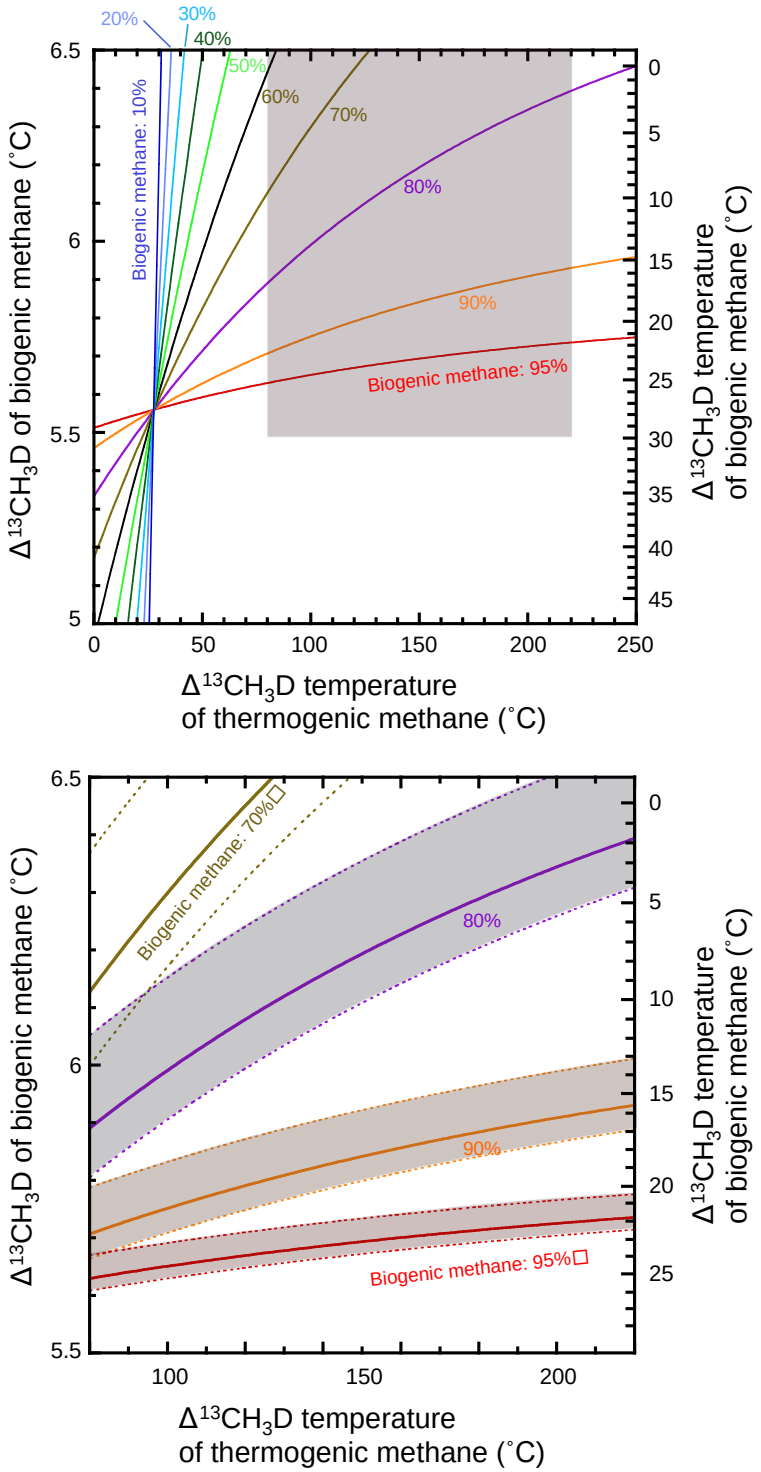

fig. S9. Mixing curves of $\Delta^{13}CH_3D$ between biogenic and thermogenic methane end-members consistent with a final clumped isotopologue temperature of 30°C for the resultant mixture. Curves show different assumed proportions of biogenic gas. X-axis is $\Delta^{13}CH_3D$ temperature for thermogenic end-member. Left Y-axis and right Y-axis indicate $\Delta^{13}CH_3D$ and $\Delta^{13}CH_3D$ temperature for biogenic end-member, respectively. Solid curve demonstrates a two end-member mixing scenario between biogenic and thermogenic hydrocarbons with varying biogenic fractions (10–95%). The lower graph is a close-up of the possible $\Delta^{13}CH_3D$ temperature of thermogenic CH_4 (pink shading in the upper graph). Dashed curves indicate the possible range of two-end-member mixing scenario (see Supplementary Methods).